Applied Energy Symposium 2021: Low carbon cities and urban energy systems
September 4-8, 2021, Matsue, Japan
Paper ID: 20

The optimal solution to increase across-tube heat transfer channel through polyethylene bridge

Lin Qiu[1*], Fengcheng Li[1], Ning Zhu[1], Yanhui Feng[1*], Xinxin Zhang[1], Xiaohua Zhang[2*]

1 School of Energy and Environmental Engineering, University of Science and Technology Beijing, Beijing 100083, China

2 Innovation Center for Textile Science and Technology, Donghua University, Shanghai 201620, China

ABSTRACT

The enormous interfacial thermal resistance between adjacent CNT leads to a significant weakening of the overall thermal conductivity of the CNT-assembled materials. In this study, based on the parallel CNT interfaces of natural van der Waals interaction, a unique scheme was proposed to enhance the interfacial thermal transport properties. The initial arrangement of polyethylene (PE) chains with linear configuration was oriental controlled and loaded to both sides of parallel CNT interfaces. The results show that the arrangement angle between PE and CNT axis has a key influence on the interfacial thermal conductance, which is conducive to the increase of effective heat transfer area between parallel CNT interfaces, and an abundant low-frequency phonon vibration mode is excited at the interfaces, so as to achieve the significant improvement of the thermal transport properties between parallel CNT interfaces (up to 120%).

Keywords: Carbon nanotube, Interfacial thermal transport, Polyethylene, Bridging effect

NONMENCLATURE

Abbreviations	
APEN	Applied Energy
Symbols	
n	Year

1. INTRODUCTION

Owing to their special one-dimensional structure and various excellent properties, such as ultra-high tensile strengths and thermal conductivities, carbon nanotube (CNTs) have been widely concerned and investigated by material scientists, especially in applications of microelectronics, aerospace, energy storage, thermal management, and so forth [1-8]. In the more applicable materials where CNTs are often assembled together to form CNT fibers, films/papers, gels, and arrays/forests, enormous intertube contacts are generated, through which both the load and heat transfers are strongly hindered by the weak van der Waals (vdW) interactions. Thus far, by optimizing the assembly structure, remarkable strengthening results have been realized for CNT fibers, films, and their composites [9-11], while the thermal conductivity of CNT assembly materials is still far below expectation and much lower than that of individual CNTs. For example, a wide range of values of 60--770 W/m·K have been measured for the apparent thermal conductivity of CNT fibers [12-16], depending on the fiber length, while the intrinsic (real) thermal conductivity is still just about 60 W/m·K for untreated CNT fibers and can be improved up to 177 W/m·K by designing a composite and compact structure using thermosetting polymers [17, 18].

Recent investigations have shown that the thermal contact resistance between parallel CNTs mainly depends on the distance, overlap length and length of CNT, crossing angle, and external pressure [19-24]. The typical value of the interfacial thermal conductance *G* is in the range of 10-100 W/m·K [19, 24], and the value between crossed CNTs is two orders of magnitude smaller than that between parallel CNTs [22]. Loading or

Selection and peer-review under responsibility of the scientific committee of CUE2021

decoration of nanoparticles at the intertube contact is considered to an effective way to improve the thermal transport performance. For example, iodine atom chains and gold nanoparticles are found to remarkably enhance the conductance due to the coupling of low-frequency phonon modes and the increased channels for heat transport [25, 26]. The covalent binding of linking molecules between CNTs can also improve the intertube conductance, however such effect decreases very rapidly, and even becomes negative, with increasing the molecular chain length [27]. The direct surface functionalization of CNTs is another effective strategy and the intertube conductance can be increased by nearly 75% [17]. However, the inherent thermal conductivity of the CNTs is greatly weakened by the functionalization. Polymer wrapping, as a new solution, is also effective for the phonon coupling at intertube contacts, and thus for the improvement of interfacial conductance. However, such enhancement is still limited by the wrapping density [28].

Due to the polymer itself is prone to agglomerate to form a network, this disordered network with lower thermal conductivity will further deteriorate the interfacial thermal transport properties. Therefore, this paper assumes that the orderly arrangement of polymers at the interface has a more significant effect on the improvement of *G* and avoids the interference of disordered polymer networks. In response to the above conjecture, this paper proposes a novel strategy to directional control the initial arrangement of polyethylene (PE) chains and load them on both sides of the parallel CNT interfaces. The *G* of parallel CNT interfaces is calculated by the non-equilibrium molecular dynamics (NEMD) method, and explored the effect of PE chains on *G* under different initial arrangements. The PE chains with good linear structure avoids the disorder and phonon scattering produced by amorphous PE in the composite material.

2. COMPUTATIONAL DETAILS

In order to describe the effect of PE bridging on the interfacial heat transfer between CNTs, two parallel and partially overlapping finite single-wall CNTs are connected to heat source and sink, respectively, and six PE molecules are placed at the groove position of the two CNTs, as shown in Figure 1a. Different contacts between two (10,10) and two (20,20) CNTs are investigated, to show the diameter dependence. The spacing of the two tube is both set to be 3.4 Å, and the overlap distance is fixed to be 40 Å. The CNT length is 246.0 and 123.0 Å for the (10,10) and (20,20) CNTs, which are found to be

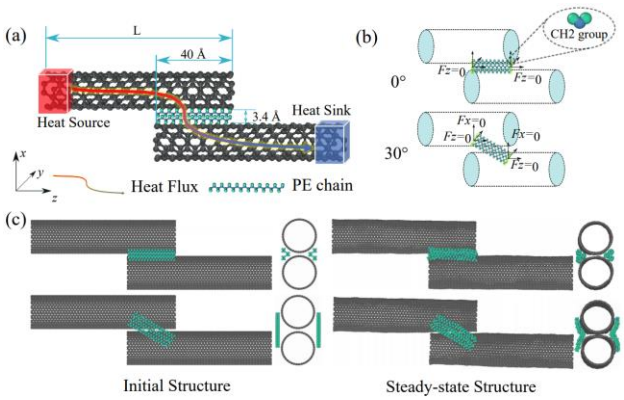

Fig 1 (a) Schematic diagram of the molecular dynamics setup used to predict the *G* of the parallel (20,20) CNT interfaces, (b) Schematic diagram of the constraint method for the initial arrangement angle of the PE chains, (c) Take 0 and 30° as an example, the schematic diagram of the initial and steady-state structure in the simulation

sufficient to establish a stable temperature gradient between them. As the CNTs are finite length, no periodic condition is used in each direction. The left 1 nm segment of the top CNT and the right 1 nm segment of the bottom CNT are connected to the heat source and sink, respectively. The PE molecules have a chain length of 40.6 Å (containing 32 sp^3-bonded C atoms), and are placed beside the CNT contact to act as a regulator for inter-tube heat conduction. To evaluate the effect of polymer orientation, the PE molecules are initially placed as straight lines at an angle with the tube axis of α=0°, 30°, 45°, 60°, and 90°, respectively (Figure 1b). The orientation is constrained by limiting the motion of the end groups in the *xy* plane for α=0°, or in the *yz* plane for the other orientation angles. Such weak constrain can still allow the full relaxation for the PE polymers, where the polymer segments can rotate and bend to contact the CNTs more tightly (Figure 1c), leading to the reduction of total energy.

The simulation is carried out by using the Large-scale Atomic/Molecular Massively Parallel Simulator (LAMMPS) package [29], and the interatomic (carbon and hydrogen) interactions in the CNTs and PE chains are described by the adaptive intermolecular reactive empirical bond-order (AIREBO) potential [30], which includes the many-body Tersoff--Brenner-style covalent interaction and the Lennard--Jones vdW interactions. The simulation timestep is set to 0.5 fs. The system is first stabilized at 300 K for a long time (0.3 ns is quite enough) by using a Nose--Hoover thermostat [31, 32], and then the Jund--Julien algorithm [33] is applied on the heat source and sink under the *NVE* ensemble. After the steady state is reached for a sufficiently long time (0.8

ns), the temperatures of each 18-Å or 10-Å segment of the (10,10) or (20,20) CNT are measured within a long time period (e.g., 0.5-1 ns).

The intertube thermal conductance (per unit length) G is calculated according to Fourier's law,

$$G=\frac{J}{L\Delta T} \quad (1)$$

where J is the magnitude of the heat flow, ΔT is the temperature difference, and L is the overlapping length. In order to clarify the underlying mechanism for thermal transport, the vibration density of states (VDOS) of the CNTs and selected carbon atoms (at the CNT contact) are calculated based on the Fourier transform from the atomic velocity auto-correlation function (VACF),

$$\mathrm{VACF}(t)=\left\langle \vec{v}(t)\cdot\vec{v}(0)\right\rangle =\frac{1}{N}\sum_{i=1}^{N}\vec{v}_i(0+t)\cdot\vec{v}_i(0) \quad (2)$$

where $\vec{v}_i(0)$ and $\vec{v}_i(t)$ are the velocity vectors of i-th atom at initial configuration and time t, respectively.

3. RESULTS AND DISCUSSION

3.1 Interfacial thermal conductance

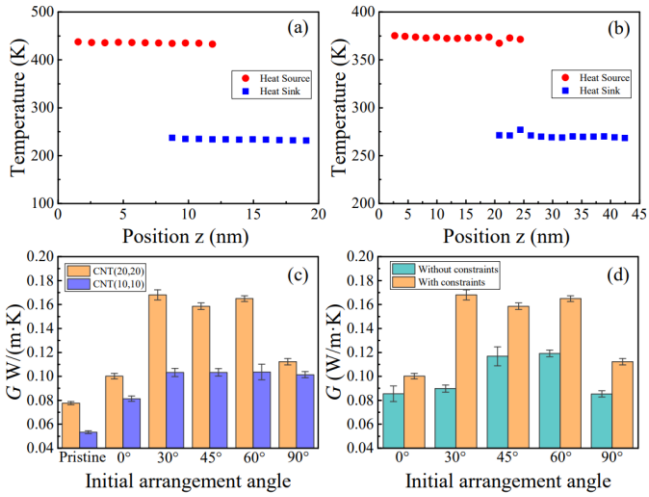

Fig 2 Typical steady-state temperature profiles in the two CNTs for (a) (10,10)/(10,10), (b) (20,20)/(20,20), (c) The evolution trend of interfacial thermal conductance with different initial arrangements of PE chains and (d) Compare the interfacial thermal conductance under different initial arrangements of PE chains with or without constraints.

By applying/extracting quantitative heat flow to the heat source and heat sink, a temperature gradient can be constructed inside the simulation system. A typical temperature curve is shown in Figure 2a and b, the temperature along each CNT is uniform, and there is only one temperature drop ΔT at the junction, which confirms that the thermal resistance within each CNT is negligible. The interfacial thermal conductance G is then obtained from temperature drop ΔT and Equation (1).

To ensure that the simulation results are sufficiently reliable, the effects of different initial arrangements in the two systems on G are calculated and compared, as shown in Figure 2c and d. At room temperature, compared with the pristine parallel CNT interfaces, the G of the directional controlled PE loaded parallel CNT interface shows an extremely amazing effect; for systems I and II, the initial arrangement angle has basically the same influence on the G. It is worth noting that when the initial arrangement angle is 30°, 45° and 60°, the improvement of G is the most significant, and the maximum improvement effect of G in the two systems is as high as 119% and 120%, respectively. It fully proves that when there is a certain angle between the PE chain and the CNT axis, it is more conducive to the improvement of G. At 0° and 90°, the improvement effect of G is not ideal.

Overall, the G of system I is significantly lower than that of system II, which is attributed to the larger diameter of CNTs with larger surface area, so that the larger effective heat transfer area between two parallel CNTs. Therefore, it can be inferred that G has a strong dependence on the diameter of CNTs, and the impact of diameter on G is dominant compared with the length of CNTs. And by appropriately increasing the CNT diameter, the coupling strength and the effective heat transfer area between CNTs can be improved. In addition, for the pristine parallel CNT interfaces with a chirality of (10, 10), G is 0.0526 W/m·K, which is consistent with the G of the parallel CNT interface with a length of 100-200 nm and a chirality of (10,10) obtained in the reference, G is 0.06

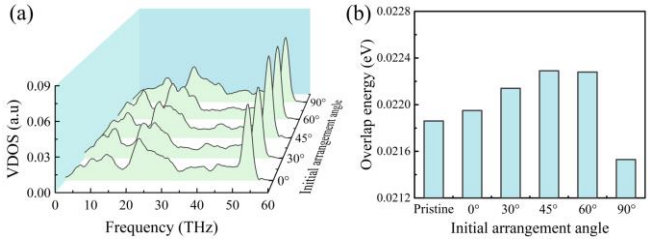

Fig 3 For different initial arrangements of PE chains, (a) Phonon VDOS of the local C atoms at the parallel CNT interfaces. (b) Phonon energy in the overlap area of VDOS between the local C atoms on both sides of the parallel CNT interface.

W/m·K [34], it is also the same as the G of the 25-75 nm long (10,10) CNT interface with an overlap length of 4-9.5 nm reported by the MD method in the literature [35],

0.05-0.08 W/m·K, which proves the accuracy of the results.

Compare the effect of the initial arrangement of PE chains on *G* of the parallel CNT interface with or without constraints, as shown in Figure 2d. The results indicate that imposing constraints on the PE chains can greatly reduce the temperature difference between the two sides of the parallel CNT interface, and significantly improve the heat transfer performance of the parallel CNT interface. For the initial arrangement angles of 30°, 45° and 60°, the improvement of the *G* is the most significant, up to 83%. When arranged at 0°, due to the number of PE chains is small (n=6), they can always be loaded on both sides of the interface in an orderly manner, which is the same as the effect of directional control of PE chains by imposing constraints, so that there is no obvious difference in *G*.

3.2 Local phonon vibration density of states and overlap energy

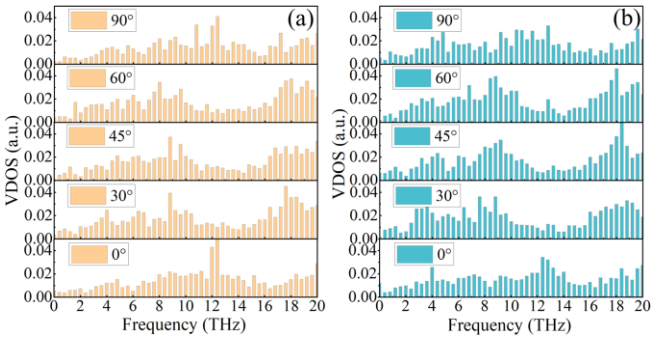

Fig 5 For different initial arrangements of PE chains, compare the VDOS of local C atoms at the parallel CNT interfaces: (a) Heat source, (b) Heat sink.

Comparing and analyzing the VDOS of local C atoms at the parallel CNT interface under different initial arrangements, it can be found that the VDOS of 0° and 90° is significantly different from other initial arrangements, and the curve in the low frequency region is relatively flat and there is no obvious peak in the low frequency region. In other cases, the peaks increase in multiple frequency regions, which reasonably explains the significant increase in *G* (Figure 4a). In addition, the overlap energy is used to quantify the phonon energy in the VDOS overlap area of the C atoms on both sides of the parallel CNT interface (the degree of overlap of the phonon VDOS of the C atoms on both sides), and the results are shown in Figure 4b. Compared with the pristine parallel CNT interface, the directional control of the initial arrangement of the PE chains enables a significant increase in the phonon energy in the overlapping area (except for the initial arrangement of 90°), and the increase in overlap energy at 30°, 45° and 90° is the most obvious, which echoes the result of the *G*. It shows that the directional control of PE chain arrangement and loading parallel CNT interface effectively improves the matching of VDOS, and increases the interfacial phonon transmission ability.

We further compared and analyzed the local phonon VDOS of C atoms at the interface under different initial arrangements (in low-frequency region, < 20 THz), as shown in Figure 5. For several different initial arrangements, there is little difference in the local VDOS between the C atoms on the “heat source”. Compared with 0 and 90°, the enhancement of the low-frequency phonon only occurs in the frequency range of 16-20 THz. Interestingly, the local phonon VDOS on the “heat sink” produces a significant difference. Similarly, the local VDOS is relatively flat at 0 and 90°, while there are abundant low-frequency phonon under other initial arrangements, which reveals that another key factor for the significant improvement of the *G* is that the C atoms on the “heat sink” are excited by a large number of low-frequency phonons (especially around 4, 8 and 18 THz), and it has a significant positive effect on interfacial thermal transport.

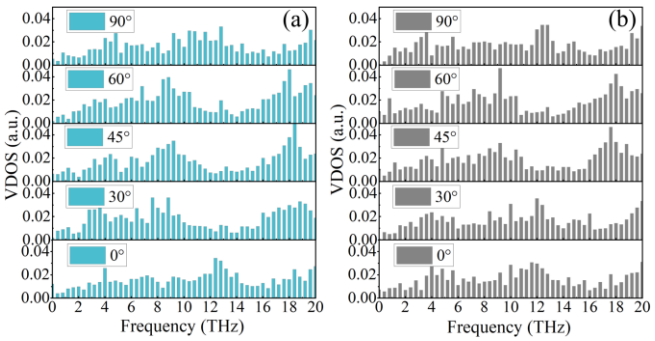

Fig 6 For different initial arrangements of PE chains, compare the VDOS of the local C atoms on the “heat sink” at the parallel CNT interfaces: (a) With constraints, (b) Without constraints.

To further clarify the internal mechanism of the impact of the the constrained PE chain on *G*, specifically for the case that the *G* is much higher than under unconstrained conditions, the local VDOS of the C atoms at the interface with or without constraints is analyzed. Similarly, there is little difference in the local phonon VDOS of the C atom on the “heat source” in the two cases. In reverse, the difference on the “heat sink” is so obvious, as shown in Figure 6. Compared without constraints, the local VDOS with constraints and the initial arrangement of 30°, 45° and 60° has more prominent low-frequency peaks and richer low-frequency phonons, thus it accurately reveals the

internal mechanism that the *G* has a significant difference in the two cases. In addition, for the initial arrangement of 0 and 90°, with or without constraints has no significant effect on the local VDOS of the carbon atoms on the "heat sink", which also indicates that the PE chains with constraints have minor effect on the *G*.

4. CONCLUSION

This paper proposes a novel method to impose constraints on PE chains and load them on both sides of the parallel CNT interfaces, and explore the effect of directional control of the initial arrangements of PE molecular chains on the *G*. Compared with the pristine parallel CNT interface, imposing constraints on the PE chains has achieved a significant increase in the *G*, and the initial arrangement of 30°, 45° and 60° has the best effect in improving the *G*, and the highest increases of about 119% and 120% are achieved in systems I and II, respectively.

It can be attributed to two aspects: firstly, the initial arrangement of PE chains by directional control leads to significant deformation of the structure at the parallel CNT interfaces, and the flat structure leads to an increase in the effective heat transfer area, which is beneficial to interface heat transfer; Secondly, the low-frequency phonon modes of the local C atoms at the parallel CNT interface is excited (the C atoms on the "heat sink" are dominant), and the phonon energy of the C atoms on both sides of the interface improves the phonon transmission ability, which is more conducive to interfacial thermal transport.

Comparing the effects of different arrangements on the *G* with or without constraints, it is found that the *G* with constraints is much higher than that without constraints (30° is the most significant). The *G* between the several arrangements is not much different without imposing constraints, indicating that the initial arrangement has negligible impact on the *G*.

The above findings put forward a novel strategy to enhance the thermal conductance of CNT-assembled materials, and promote the development of ultra-high thermal conductivity nano-assembled materials in the future, and provide important theoretical guidance for industrial applications of efficient thermal management in the fields of microelectronics and nano energy.

ACKNOWLEDGEMENT

The authors are grateful for the financial support from the Beijing Natural Science Foundation (3202020), National Natural Science Foundation of China (51876008), Beijing Nova Program (Z201100006820065) and Fundamental Research Funds for the Central Universities (2232021G-01).

REFERENCE

[1] Van der Geer J, Hanraads JAJ, Lupton RA. The art of writing a scientific article. J Sci Commun 2010; 163:51–9. (Reference to a journal publication)

[2] Strunk Jr W, White EB. The elements of style. 4th ed. New York: Longman; 2000. (Reference to a book)

[3] Mettam GR, Adams LB. How to prepare an electronic version of your article. In: Jones BS, Smith RZ, editors. Introduction to the electronic age, New York: E-Publishing Inc; 2009, p. 281–304. (Reference to a chapter in an edited book)

[1] Baughman RH, Zakhidov AA, de Heer WA. Carbon Nanotubes -- the Route Toward Applications. Science 2002; 297:787-792

[2] Segal D, Nitzan A, Hänggi P. Thermal conductance through molecular wires. J Chem Phys 2003; 119:6840-6855.

[3] Balandin AA. Thermal properties of graphene and nanostructured carbon materials. Nat Mater 2011; 10:569-581.

[4] Jiang H. Chemical preparation of graphene-based nanomaterials and their applications in chemical and biological sensors. Small 2011; 7:2413-2427.

[5] Qiu L, Zhu N, Zou H, Feng Y, Zhang X, Tang D. Advances in thermal transport properties at nanoscale in China. Int J Heat Mass Transfer 2018; 125:413-433.

[6] Qiu L, Zhu N, Zou H, Feng Y, Michaelides EE, Żyła G, Jing D, Zhang X, Norris PM, Markides CN, Mahian O. A review of recent advances in thermophysical properties at the nanoscale: From solid state to colloids. Phys Rep 2020; 843:1-81.

[7] Qiu L, Ouyang Y, Feng Y, Zhang X. Review on micro/nano phase change materials for solar thermal applications. Renew Energ 2019; 140:513-538.

[8] Xu W, Chen Y, Zhan H, Wang JN. High-Strength Carbon Nanotube Film from Improving Alignment and Densification. Nano Lett 2016; 16:946-952.

[9] Jung Y, Cho YS, Lee JW, Oh JY, Park CR. How can we make carbon nanotube yarn stronger? Compos Sci Technol 2018; 166:95-108.

[10] Zhang X, Lu W, Zhou G, Li Q. Understanding the Mechanical and Conductive Properties of Carbon Nanotube Fibers for Smart Electronics. Adv Mater 2020; 32:1902028.

[11] Jakubinek MB, Johnson MB, White MA, Jayasinghe C, Li G, Cho W, Schulz MJ, Shanov V. Thermal and

electrical conductivity of array-spun multi-walled carbon nanotube yarns. Carbon 2012; 50:244-248.
[12] Behabtu N, Young CC, Tsentalovich DE, Kleinerman O, Wang X, Ma AWK, Bengio EA, ter Waarbeek RF, de Jong JJ, Hoogerwerf RE, Fairchild SB, Ferguson JB, Maruyama B, Kono J, Talmon Y, Cohen Y, Otto MJ, Pasquali M. Strong, Light, Multifunctional Fibers of Carbon Nanotubes with Ultrahigh Conductivity. Science 2013; 339:182-186.
[13] Mayhew E, Prakash V. Thermal conductivity of high performance carbon nanotube yarn-like fibers. Appl Phys Lett 2014; 115:174306.
[14] Liu P, Fan Z, Mikhalchan A, Tran TQ, Jewell D, Duong HM, Marconnet AM. Continuous Carbon Nanotube-Based Fibers and Films for Applications Requiring Enhanced Heat Dissipation. ACS Appl Mater Interfaces 2016; 8:17461-17471.
[15] Gspann TS, Juckes SM, Niven JF, Johnson MB, Elliott JA, White MA, Windle AH. High thermal conductivities of carbon nanotube films and micro-fibres and their dependence on morphology. Carbon 2017; 114:160-168.
[16] Qiu L, Wang X, Tang D, Zheng X, Norris PM, Wen D, Zhao J, Zhang X, Li Q. Functionalization and densification of inter-bundle interfaces for improvement in electrical and thermal transport of carbon nanotube fibers. Carbon 2016; 105:248-259.
[17] Qiu L, Guo P, Yang X, Ouyang Y, Feng Y, Zhang X, Zhao J, Zhang X, Li Q. Electro curing of oriented bismaleimide between aligned carbon nanotubes for high mechanical and thermal performances. Carbon 2019; 145:650-657.
[18] Foygel M, Morris RD, Anez D, French S, Sobolev VL. Theoretical and computational studies of carbon nanotube composites and suspensions: Electrical and thermal conductivity. Phys Rev B 2005; 71:104201.
[19] Zhong H, Lukes JR. Interfacial thermal resistance between carbon nanotubes: Molecular dynamics simulations and analytical thermal modeling. Phys Rev B 2006; 74:125403.
[20] Chalopin Y, Volz S, Mingo N. Upper bound to the thermal conductivity of carbon nanotube pellets. J Appl Phys 2009; 105:084301.
[21] Yang J, Waltermire S, Chen Y, Zinn AA, Xu TT, Li D. Contact thermal resistance between individual multiwall carbon nanotubes. Appl Phys Lett 2010; 96:023109.
[22] Evans WJ, Shen M, Keblinski P. Inter-tube thermal conductance in carbon nanotubes arrays and bundles: Effects of contact area and pressure. Appl Phys Lett 2012; 100:261908.
[23] Hu GJ, Cao BY. Thermal resistance between crossed carbon nanotubes: Molecular dynamics simulations and analytical modeling. J Appl Phys 2013; 114:224308.
[24] Qiu L, Zou H, Zhu N, Feng Y, Zhang X, Zhang X. Iodine nanoparticle-enhancing electrical and thermal transport for carbon nanotube fibers. Appl Therm Eng 2018; 141:913-920.
[25] Qiu L, Zou H, Wang X, Feng Y, Zhang X, Zhao J, Zhang X, Li Q. Enhancing the interfacial interaction of carbon nanotubes fibers by Au nanoparticles with improved performance of the electrical and thermal conductivity. Carbon 2019; 141:497-505.
[26] Varshney V, Patnaik SS, Roy AK. Modeling of Thermal Conductance at Transverse CNT-CNT Interfaces J Phys Chem C 2010; 114:16223-16228.
[27] Xu Z, Buehler MJ. Nanoengineering Heat Transfer Performance at Carbon Nanotube Interfaces. ACS Nano 2009; 3:2767-2775.
[28] Plimpton S. Fast Parallel Algorithms for Short-Range Molecular Dynamics. J Comput Phys 1995; 117:1-19.
[29] Stuart SJ, Tutein AB, Harrison JA. A Reactive Potential for Hydrocarbons with Intermolecular Interactions. J Chem Phys 2000; 112:6472-6486.
[30] Nosé S. A unified formulation of the constant temperature molecular dynamics methods. J Chem Phys 1984; 81:511-511.
[31] Hoover WG. Canonical Dynamics: Equilibrium Phase-Space Distributions. Phys Rev A 1985; 31:1695-1697.
[32] Jund P, Jullien R. Molecular-dynamics calculation of the thermal conductivity of vitreous silica. Phys Rev B 2007; 59:13707-13711.
[33] Volkov AN, Salaway RN, Zhigilei LV. Atomistic simulations, mesoscopic modeling, and theoretical analysis of thermal conductivity of bundles composed of carbon nanotubes. J Appl Phys 2013; 114:104301.
[34] Liao Q, Liu Z, Liu W, Deng C, Yang N. Extremely High Thermal Conductivity of Aligned Carbon Nanotube-Polyethylene Composites. Sci Rep 2015; 5:16543.